BIOCHEMISTRY
including biophysical chemistry & molecular biology

Article

pubs.acs.org/biochemistry

Fundamental Reaction Pathway and Free Energy Profile for Butyrylcholinesterase-Catalyzed Hydrolysis of Heroin

Yan Qiao,[†,‡] Keli Han,*[,†] and Chang-Guo Zhan*[,‡]

[†]State Key Laboratory of Molecular Reaction Dynamics, Dalian Institute of Chemical Physics, Chinese Academy of Science, Zhongshan Road 457, Dalian 116023, P. R. China

[‡]Department of Pharmaceutical Sciences, College of Pharmacy, University of Kentucky, 789 South Limestone Street, Lexington, Kentucky 40536, United States

ABSTRACT: The pharmacological function of heroin requires an activation process that transforms heroin into 6-monoacetylmorphine (6-MAM), which is the most active form. The primary enzyme responsible for this activation process in human plasma is butyrylcholinesterase (BChE). The detailed reaction pathway of the activation process via BChE-catalyzed hydrolysis has been explored computationally, for the first time, in this study via molecular dynamics simulation and first-principles quantum mechanical/molecular mechanical free energy calculations. It has been demonstrated that the whole reaction process includes acylation and deacylation stages. The acylation consists of two reaction steps, i.e., the nucleophilic attack on the carbonyl carbon of the 3-acetyl group of heroin by the hydroxyl oxygen of the Ser198 side chain and the dissociation of 6-MAM. The deacylation also consists of two reaction steps, i.e., the nucleophilic attack on the carbonyl carbon of the acyl−enzyme intermediate by a water molecule and the dissociation of the acetic acid from Ser198. The calculated free energy profile reveals that the second transition state (TS2) should be rate-determining. The structural analysis reveals that the oxyanion hole of BChE plays an important role in the stabilization of rate-determining TS2. The free energy barrier (15.9 ± 0.2 or 16.1 ± 0.2 kcal/mol) calculated for the rate-determining step is in good agreement with the experimentally derived activation free energy (~16.2 kcal/mol), suggesting that the mechanistic insights obtained from this computational study are reliable. The obtained structural and mechanistic insights could be valuable for use in the future rational design of a novel therapeutic treatment of heroin abuse.

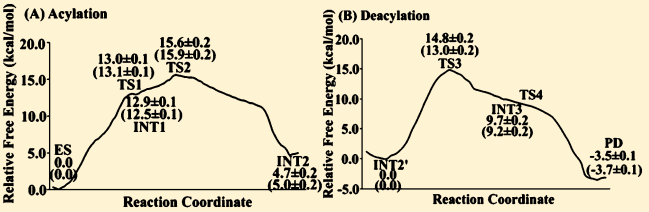

Heroin (3,6-diacetylmorphine) is an illegal, highly addictive opiate drug.[1] Heroin produces euphoria or pleasurable feelings. A pleasurable euphoria feeling is usually followed by a drowsy feeling for several hours because of the depression of the central nervous system (CNS). Because of the drowsy feeling and depression of the CNS, the drug may impair judgment and memory and cloud mental functioning.

Heroin is the most abused of the opiates.[1] For example, in 2011, 4.2 million Americans reported using heroin at some time in their lives, and 23% of the individuals were classified as being dependent on or abusing heroin.[1] Heroin abuse can result in serious health problems, including miscarriages, heart infections, and even death. In addition, heroin abuse also has repercussions that extend far beyond the individual users. The medical and social consequences of heroin abuse include transmission of HIV/AIDS, tuberculosis, crime, violence, and disruptions in family, workplace, and educational environments. These consequences have a devastating impact on our society and cost billions of dollars per year.[1] The disastrous medical and social consequences of heroin addiction have made the development of an effective pharmacological treatment of heroin abuse a high priority.

Heroin is also the most rapidly acting of the opiates.[2] However, heroin actually has a very low μ-opioid receptor binding affinity, and thus, heroin itself has a low potency in activating the G-protein to produce its effects on neurotransmitter systems.[3] Nevertheless, once injected, heroin is very rapidly metabolized via hydrolysis to 6-monoacetylmorphine (6-MAM) (Scheme 1), which can readily cross the blood−brain barrier (BBB) and be rapidly concentrated in the brain.[4−6] More importantly, 6-MAM has a higher μ-opioid receptor affinity than its precursor heroin.[3] It has been recognized that heroin acts principally via 6-MAM.[3,7−10]

Scheme 1. BChE-Catalyzed Hydrolysis of Heroin to 6-MAM

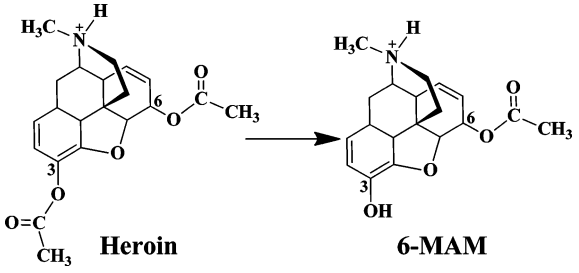

Received: June 5, 2013
Revised: August 15, 2013
Published: August 30, 2013

   dx.doi.org/10.1021/bi400709v | *Biochemistry* 2013, 52, 6467−6479

These pharmacological characteristics of heroin suggest that heroin actually behaves as a prodrug.[11,12] The prodrug is metabolized into 6-MAM, which is actually the most potent form of the drug responsible for the main pharmacological effects of heroin. From this point of view, the hydrolysis of heroin to 6-MAM may be regarded as an activation process, i.e., the activation of heroin itself, which transforms heroin (a relatively inactive form) into 6-MAM (the most active form).

With regard to the endogenous enzymes responsible for the activation process, while carboxylesterases 1 and 2 (hCE-1 and hCE-2, respectively) in liver and brain can catalyze the hydrolysis of heroin to 6-MAM,[13] serum butyrylcholinesterase (BChE) and erythrocyte acetylcholinesterase (AChE) can also hydrolyze heroin to 6-MAM in blood.[9,13,14] Although many tissues have the ability to hydrolyze heroin, blood is generally the first to act on heroin.[9] According to the results of Boix et al.,[15] it is the high blood metabolic rate of heroin and the good BBB permeability of 6-MAM, rather than heroin itself, that could account for the highly efficient delivery of the active metabolites to the brain after heroin is administered. The experimental results reported by Lockridge et al.[9] also indicated that serum should be the major site of 6-MAM production. In comparison, human serum BChE can hydrolyze heroin to 6-MAM with a reaction rate of 4.5 μmol L^{-1} min^{-1}, which is 9-fold greater than the heroin hydrolysis rate (0.5 μmol L^{-1} min^{-1}) by human erythrocyte AChE.[14] Therefore, BChE should be the major enzyme hydrolyzing heroin to 6-MAM in the human body. Because BChE can hydrolyze heroin to 6-MAM efficiently with a high catalytic rate constant (k_{cat} = 540 min^{-1}),[14] the half-life of heroin itself in human is only ~2−5 min.[14,16−18] In comparison, 6-MAM has a much longer half-life (up to 52 min) in the human body.[19]

On the basis of the background described above, it is interesting in terms of understanding the molecular mechanism of heroin abuse to uncover the detailed catalytic mechanism concerning how human BChE hydrolyzes heroin to 6-MAM and thus activates heroin. A detailed understanding of the molecular mechanism could provide valuable mechanistic clues for the rational design of a novel therapeutic treatment of heroin abuse.

In this study, the detailed reaction pathway for BChE-catalyzed hydrolysis of heroin to 6-MAM has been explored, for the first time, by performing molecular dynamics (MD) simulation and first-principles quantum mechanical/molecular mechanical free energy (QM/MM-FE) calculations.[20−23] In the QM/MM-FE calculations, first-principles QM/MM reaction-coordinate calculations were followed by free energy perturbation (FEP) calculations to account for the dynamic effects of the protein environment on the free energy profile for the catalytic reaction process. Our QM/MM calculations are based on the pseudobond first-principles QM/MM approach,[20−23] which has been demonstrated to be a powerful tool in simulating a variety of enzymes,[24−35] and some theoretical predictions have been confirmed by subsequent experimental studies.[28,35] The computational results clearly reveal the detailed reaction pathway and the corresponding free energy profile for BChE-catalyzed hydrolysis of heroin. On the basis of the calculated free energy profile for the favorable reaction pathway of the BChE-catalyzed hydrolysis process, we were able to identify the rate-determining step and understand the roles of essential residues in light of the QM/MM-optimized geometries.

COMPUTATIONAL METHODS

Preparation of the Initial Structure of the Reaction System. The initial enzyme−substrate (ES) structure was constructed from the X-ray crystal structure of human BChE [Protein Data Bank (PDB) entry 2XQF][36] and the optimized structure of heroin.[37] Initially, the geometry of heroin was optimized at the HF/6-31G* level using Gaussian03.[38] Then, the optimized geometry of heroin was used to calculate the electrostatic potential distribution on the molecular surface at the same HF/6-31G* level. The calculated electrostatic potential distribution was used to determine the partial atomic charges by using the standard restrained electrostatic potential (RESP) fitting procedure[39,40] implemented in the Antechamber module of AMBER11.[41] The determined RESP charges of the heroin atoms were used in the MD simulations described below.

To construct a reasonable binding structure of BChE binding with heroin, molecular docking and MD simulations were performed. Heroin was docked into the active site of BChE by using AutoDock version 4.0.[42] The docking process started from a conformational search by using the Solis and Wets local search method and the Lamarkian genetic algorithm (LGA) that was used to deal with the BChE−heroin interactions. The grid size used in the docking was 60 × 60 × 60 with a grid space of 0.375 Å (default). The docked enzyme−ligand complex structure was selected according to the binding energy.

The complex structure of BChE binding with heroin obtained from the molecular docking was used as the starting structures for the energy minimization and MD simulation using the Sander module of AMBER11.[41] The AMBER ff03 force field[43] was used for protein, and the general AMBER force field (gaff)[44] was used for heroin in the energy minimization and MD simulation. The BChE−heroin binding complex was first solvated in an orthorhombic box of TIP3P water molecules[45] with a minimal solute−wall distance of 10 Å and neutralized by adding one chloride ion. The final system size was ~103 Å × ~116 Å × ~119 Å, composed of 71173 atoms. The solvated system was subjected to energy minimization using AMBER11 with a nonbonded cutoff of 10 Å and a conjugate gradient energy minimization method. The energy minimization was performed first for 20000 steps for the water molecules and then 6000 steps for the backbone atoms, followed by an additional 20000 steps for the side chain atoms of the enzyme together with water molecules. Finally, the whole system was energy-minimized until a convergence criterion of 0.001 kcal mol^{-1} $Å^{-1}$ was achieved.

Starting from the energy-minimized complex structure, MD simulation was performed by using the Sander module of AMBER11.[41] The energy-minimized complex structure was gradually heated to 300 K by using the weak-coupling method with a constrained force constant of 50 kcal mol^{-1} $Å^{-2}$ on the backbone of BChE. The constrained force constant was gradually decreased during a 600 ps equilibration and finally removed for the production MD simulation. Throughout the MD simulation, a 10 Å nonbonded interaction cutoff was used and the nonbonded list was updated once every 1000 steps. The particle mesh Ewald (PME) method[46] was applied to the calculation of the long-range electrostatic interactions. During the MD simulation, the SHAKE algorithm[47] was used to fix the lengths of covalent bonds involving a hydrogen atom, allowing the use of a 2 fs time step to numerically integrate the equations of motion. The production MD run was kept for 2 ns with a

dx.doi.org/10.1021/bi400709v | Biochemistry 2013, 52, 6467−6479

Scheme 2. Fundamental Reaction Pathway for BChE-Catalyzed Hydrolysis of Heroin to 6-MAM[a]

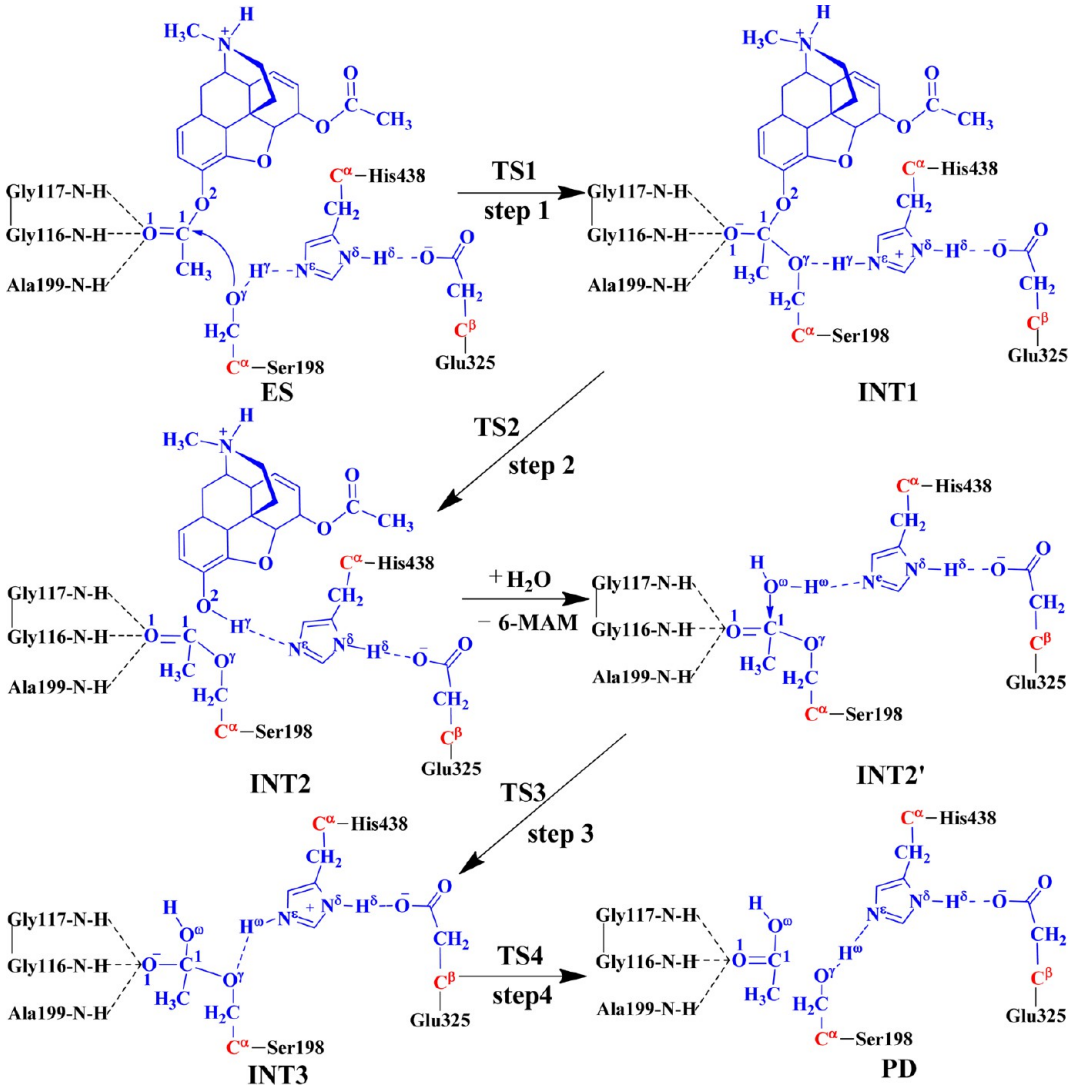

[a]The atoms colored blue belong to the QM subsystem; the atoms colored red are treated with the improved pseudobond parameters, and the other atoms belong to the MM subsystem in the pseudobond first-principles QM/MM calculations.

periodic boundary condition in the *NTP* ensemble at 300 K using Berendsen temperature coupling and at 1 atm using anisotropic molecule-based scaling.

As seen in Scheme 2, there are two reaction stages (acylation and deacylation) in the BChE-catalyzed hydrolysis of heroin. The reaction product 6-MAM leaves the protein after the acylation stage. Consequently, the initial structure of INT2′ was constructed by removing the 6-MAM from the QM/MM-optimized INT2 structure. The constructed INT2′ structure was then relaxed by performing an ∼2 ns MD simulation. The simulated INT2′ system was solvated in an orthorhombic box of TIP3P water molecules,[45] with a minimal solute−wall distance of 10 Å.

For each reaction stage (acylation or deacylation), the last snapshot of the MD simulation was used to prepare the pseudobond first-principles QM/MM calculation as we noted that the structure of the last snapshot was close to the average structure simulated. As we are mainly interested in the reaction center, the water molecules more than 50 Å from the hydroxy oxygen (O^{γ}) of Ser198 were removed. Thus, the QM/MM system consisted of 3760 water molecules and a total of 19696 atoms for the acylation, and 4232 water molecules and a total of 21065 atoms for the deacylation. The QM/MM partition strategy was based on the treatment in previous QM/MM calculations of the hydrolysis reactions of other substrates catalyzed by BChE or another serine esterase.[23,24,26,28,48] The QM subsystem in the acylation stage consisted of heroin and the catalytic triad (side chains of Ser198, His438, and Glu325), whereas the QM subsystem in the deacylation stage included the reactive water molecule and side chains of acetyl-Ser198, His438, and Glu325. A pseudobond approach[20−23] was used to deal with the QM−MM interface (see below for the used boundary of the QM−MM system). For QM/MM geometry optimization on each state of the reaction system, the initial geometry was energy-minimized first with the MM method by using AMBER11[41] until a convergence criterion for an energy gradient of 0.1 kcal mol^{-1} $Å^{-1}$ was achieved.

Minimal Energy Path of the Reaction. With a reaction-coordinate driving method and an iterative energy minimization procedure,[21] the enzymatic reaction path was determined by performing the pseudobond QM/MM calculations at the B3LYP/6-31G*:AMBER level. Specifically, the QM calcula-

dx.doi.org/10.1021/bi400709v | *Biochemistry* 2013, 52, 6467−6479

tions were performed with the B3LYP functional[49−51] and 6-31G* basis set by using a modified version of Gaussian03,[38] and the MM calculations were conducted by using a modified version of AMBER8.[52] Normal mode analysis was performed to characterize the geometries optimized for the reactant, intermediates, transition sates, and final product of the reaction process. The QM/MM-optimized structures were used to perform single-point QM/MM energy calculations with the QM part performed at the B3LYP/6-31++G** level. The B3LYP functional has been used extensively in previous QM/MM calculations on enzymatic reaction systems by many researchers, including our own group,[25,27,31,33,34,53,54] and the calculated results are generally in good agreement with the experimental data. For comparison, the QM part of the single-point QM/MM energy calculations was also performed at the B3LYP/6-31+G* and B3LYP/6-311++G** levels for the rate-determining step. In the QM/MM calculations, the boundary carbon atoms were treated with previously improved pseudobond parameters,[20−23] and no cutoff was applied to the nonbonded interactions. The convergence criterion used in the geometry optimization on the QM subsystem was the same as the original Gaussian03 default, and the convergence criterion used in the geometry optimization of the MM subsystem was that the root-mean-square deviation (rmsd) of the energy gradient is $\leq$0.1 kcal mol^{-1} Å^{-1}. In all QM/MM geometry optimizations, the atoms within 20 Å of the O$^{\gamma}$ atom of the Ser198 side chain (Scheme 2) were allowed to move while all the other atoms outside this range were frozen, and the QM and MM subsystems were energy-minimized iteratively. For each iteration step of the QM/MM geometry optimization, the MM subsystem was energy-minimized while the QM subsystem was kept frozen, whereas the QM subsystem was energy-minimized while the MM subsystem was kept frozen.

Free Energy Perturbation. Free energy perturbation (FEP) is known as a reliable computational method in combination with MD or Monte Carlo (MC) simulation in evaluating the free energy change caused by a small structural change.[55−58] This method has been used extensively in computational studies of organic reactions,[55,58−60] protein−ligand interaction,[61−66] and protein stability.[67,68] In this study, after the minimal energy path was determined by the QM/MM calculations, the free energy changes associated with the QM−MM interactions were evaluated using the FEP method.[21] The sampling of the MM subsystem was performed with the QM subsystem frozen at each state along the reaction path in the FEP calculations. During the FEP calculations, the used atomic point charges on the frozen QM atoms were determined by fitting the electrostatic potential (ESP) in the QM part of the QM/MM single-point calculations. The total free energy change from the reactant to the transition state was evaluated by using the same procedure that was used in our previous computational studies of other enzymatic reaction systems.[24−34] Using our own version of the FEP implementation,[24] the FEP calculations allowed us to more reasonably evaluate the relative free energy changes caused by the QM−MM interactions. The final relative free energy predicted by the QM/MM-FE calculations was the QM part of the QM/MM energy (excluding the Coulombic interaction energy between the point charges of the MM atoms and the ESP charges of the QM atoms) and the relative free energy change obtained from the FEP calculations at 298.15 K. The time step used in the FEP calculations was 2 fs, and the lengths of all covalent bonds involving a hydrogen atom were constrained. Each MD-based FEP calculation consisted of equilibration for 50 ps and sampling for 300 ps.

All of the MD simulations and QM/MM-FE calculations were performed on a Dell supercomputer (X-series Cluster with 384 nodes or 4768 processors) at the University of Kentucky's Computer Center. The other modeling and computations were performed on SGI Fuel workstations in our own laboratory at the University of Kentucky.

RESULTS AND DISCUSSION

BChE−Heroin Binding Structure from MD Simulation. The docked BChE−heroin complex structure revealed that the 3-acetyl group of heroin was positioned in the oxyanion hole consisting of Gly116, Gly117, and Ala199, and the positively charged amino group was positioned in the choline binding site near Trp82. Further energy minimizations and an ~2 ns MD simulation were performed on the docked enzyme−substrate (ES) complex to refine the BChE−heroin binding structure. Depicted in Figure 1 are plots of the key internuclear distances

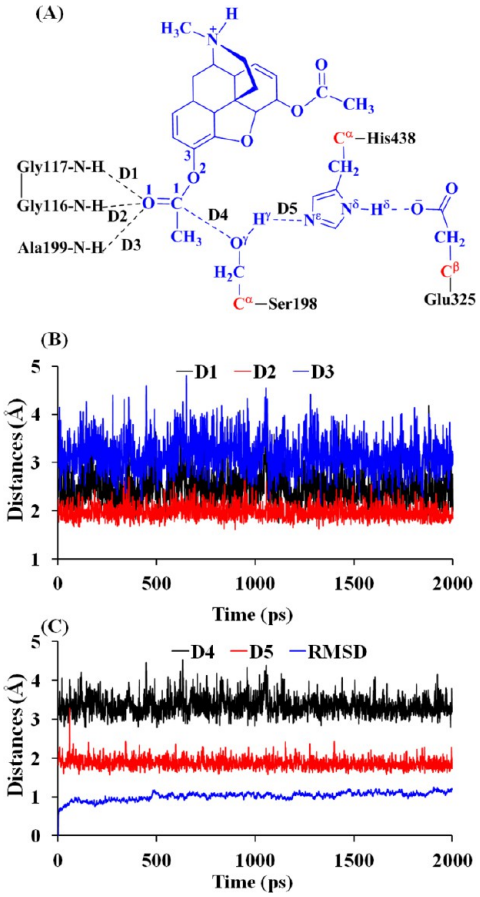

Figure 1. Plots of key internuclear distances and rmsd vs simulation time in the MD-simulated ES structure.

and the rmsd of the positions of the all backbone atoms versus the simulation time in the MD-simulated ES complex. Traces D_1−D_3 represent the internuclear distances between the carbonyl O^1 atom of the 3-acetyl group of heroin and the backbone NH hydrogen atoms of residues Gly116, Gly117, and Ala199, respectively. Trace D_4 refers to the internuclear distance between the hydroxyl O$^{\gamma}$ atom of the Ser198 side chain and the carbonyl C^1 atom of the 3-acetyl group of heroin,

dx.doi.org/10.1021/bi400709v | Biochemistry 2013, 52, 6467−6479

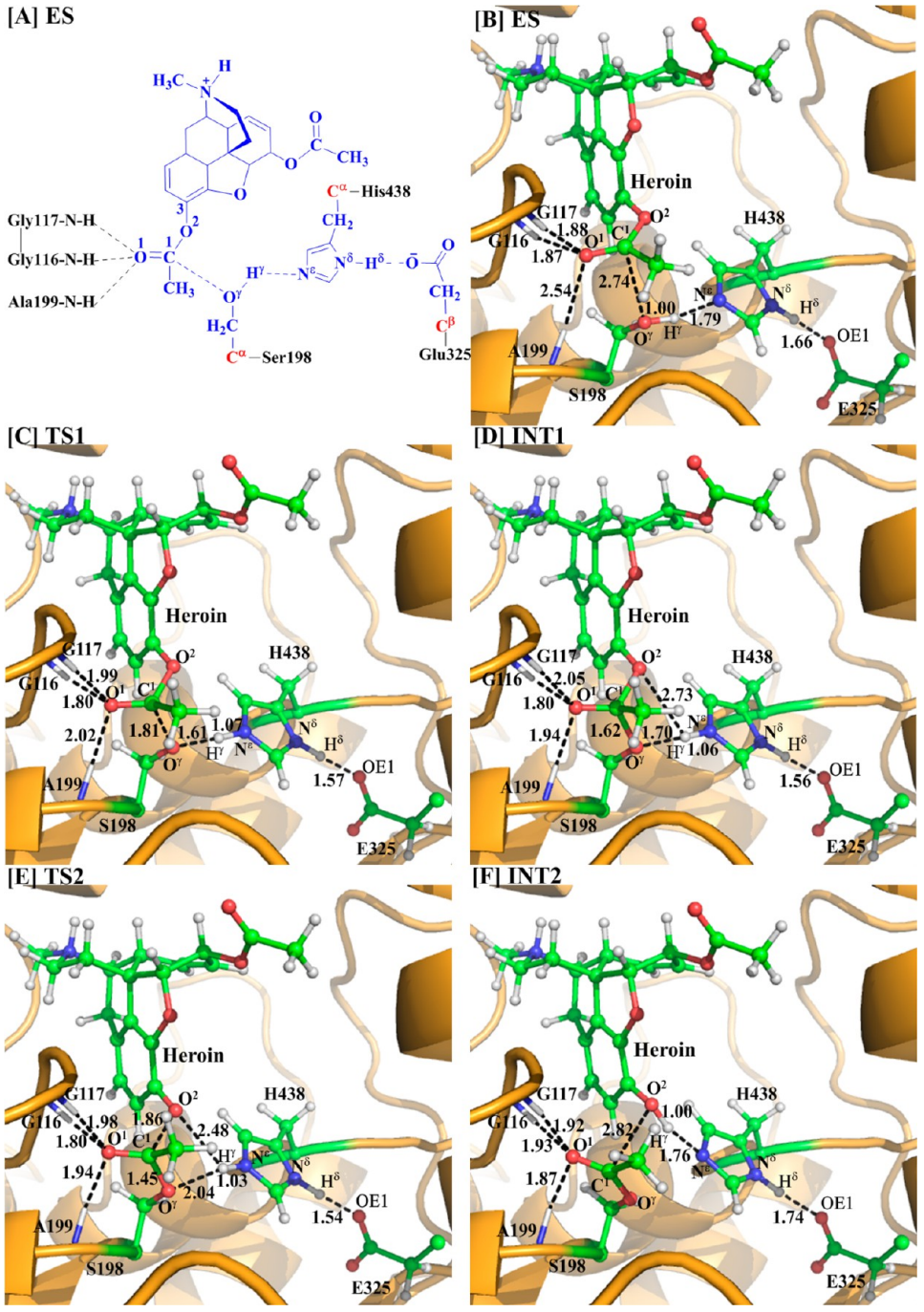

Figure 2. (A) Division of the QM/MM system. Atoms colored blue belong to the QM subsystem; the boundary carbon atoms colored red were treated with the pseudobond parameters, and all of the other atoms were included in the MM subsystem. (B–F) Geometries optimized at the QM/MM(B3LYP/6-31G*:AMBER) level for the key states during the acylation stage of the BChE-catalyzed hydrolysis of heroin. The key distances indicated in the figures are given in angstroms. The carbon, oxygen, nitrogen, and hydrogen atoms are colored green, red, blue, and white, respectively. Represented as balls and sticks are the QM atoms, with the surrounding residues rendered as sticks and the protein rendered as a cartoon.

and trace D_5 represents the internuclear distance between the hydroxyl H^{γ} atom of the Ser198 side chain and the N^{ε} atom of the His438 side chain.

As seen in Figure 1B, in the MD-simulated ES complex structure, the average values of D_1, D_2, and D_3 are 2.49, 1.97, and 3.10 Å, respectively, indicating that only two hydrogen bonds are formed between the carbonyl oxygen of the 3-acetyl group of heroin and the oxyanion hole (consisting of the backbone NH groups of Gly116, Gly117, and Ala199). As shown in Figure 1C, the average value (3.35 Å) of D_4 indicates that the hydroxyl O^{γ} atom of the Ser198 side chain is in an appropriate position to initiate the nucleophilic attack on C^1 of heroin. The average value of D_5 is 1.87 Å, showing that a strong hydrogen bond is formed between the hydroxyl group of the Ser198 side chain and the N^{ε} atom of the His438 side chain. The rmsd of the positions of all backbone atoms from those in the initial structure was also monitored to represent the overall conformational change of the protein during the MD

dx.doi.org/10.1021/bi400709v | *Biochemistry* 2013, 52, 6467–6479

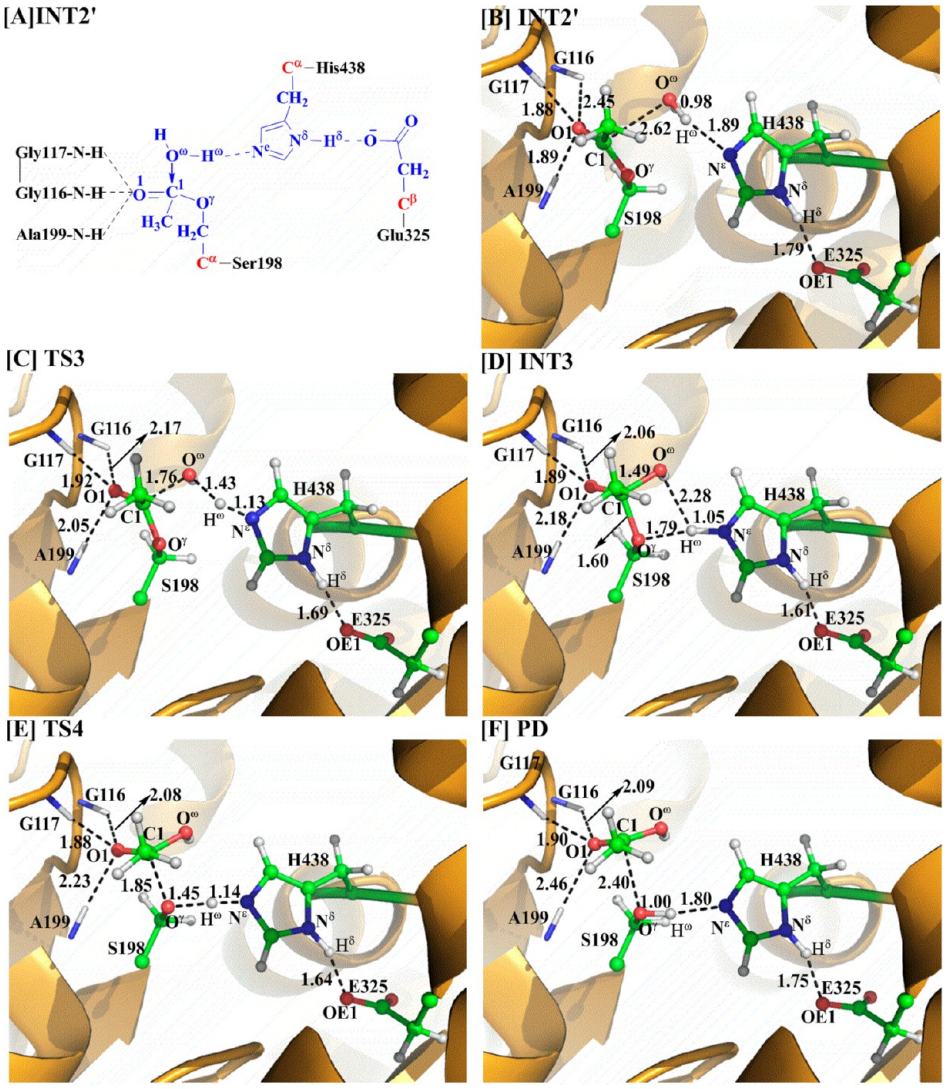

Figure 3. Geometries optimized at the QM/MM(B3LYP/6-31G*:AMBER) level for the key states of the reaction system in the deacylation stage of the BChE-catalyzed hydrolysis of heroin. The color code used here is the same as that in Figure 2.

simulation. As shown in Figure 1C, the MD trajectory was stabilized at ~100 ps, suggesting that 2 ns is long enough for the MD simulation on the ES complex.

Reaction Pathway for the BChE-Catalyzed Hydrolysis of Heroin to 6-MAM. As shown in panels B and C of Figure 1, the MD simulation led to a dynamically stable ES complex structure. The QM/MM reaction-coordinate calculations at the B3LYP/6-31G*:AMBER level starting from the MD-simulated ES complex structure revealed that the BChE-catalyzed heroin hydrolysis reaction pathway should consist of four reaction steps. The whole reaction is initiated by the nucleophilic attack of O^{γ} of the Ser198 side chain on the carbonyl C^1 atom of heroin, followed by the dissociation of the acetyl−enzyme intermediate from 6-MAM. Then, a water molecule initiates the nucleophilic attack on the carbonyl carbon (C^1) of the acylated Ser198. Finally, the dissociation of the acetic acid regenerates Ser198 of BChE. The QM/MM-optimized structures of the reactant, intermediates, transition states, and final product are depicted in Figure 2. Below we discuss each of the reaction steps in detail.

Initial Nucleophilic Attack on the Carbonyl Carbon of Heroin (step 1). The initial structure of the ES complex was first optimized at the QM/MM(B3LYP/6-31G*:AMBER) level prior to the reaction-coordinate calculations. As shown in Figure 2B for the QM/MM-optimized ES structure, D_1, D_2, and D_3 are 1.88, 1.87, and 2.54 Å, respectively, suggesting that two strong hydrogen bonds are formed between the carbonyl O^1 atom of heroin and the oxyanion hole. One is between the backbone NH group of Gly116 and O^1 of heroin, and the other is between the NH group of Gly117 and O^1 of heroin. In comparison, D_3 = 2.54 Å, indicating that the interaction between the backbone NH group of Ala199 and the carbonyl O^1 atom of heroin is much weaker.

The nucleophilic attack process proceeds as the hydroxyl O^{γ} atom of the Ser198 side chain gradually approaches the carbonyl C^1 atom of heroin, while the hydroxyl H^{γ} atom of Ser198 gradually transfers to the N^{ε} atom of the His438 side chain. This reaction step involves the breaking of the $H^{\gamma}-O^{\gamma}$ bond and the formation of both the $H^{\gamma}-N^{\varepsilon}$ and C^1-O^{γ} bonds, as shown in Scheme 2. Therefore, the changes in the $H^{\gamma}-O^{\gamma}$ ($R_{H^{\gamma}-O^{\gamma}}$), $H^{\gamma}-N^{\varepsilon}$ ($R_{H^{\gamma}-N^{\varepsilon}}$), and C^1-O^{γ} ($R_{C^1-O^{\gamma}}$) distances can reflect the nature of reaction step 1. Therefore, $R_{H^{\gamma}-O^{\gamma}} - R_{H^{\gamma}-N^{\varepsilon}} - R_{C^1-O^{\gamma}}$ was used as the reaction coordinate in the QM/MM reaction-coordinate calculations for this reaction step. As shown

dx.doi.org/10.1021/bi400709v | *Biochemistry* 2013, 52, 6467−6479

Scheme 3. Possible Reaction Pathway in the Deacylation Stage via Hypothetical Transition State TS3a with a Four-Membered Ring

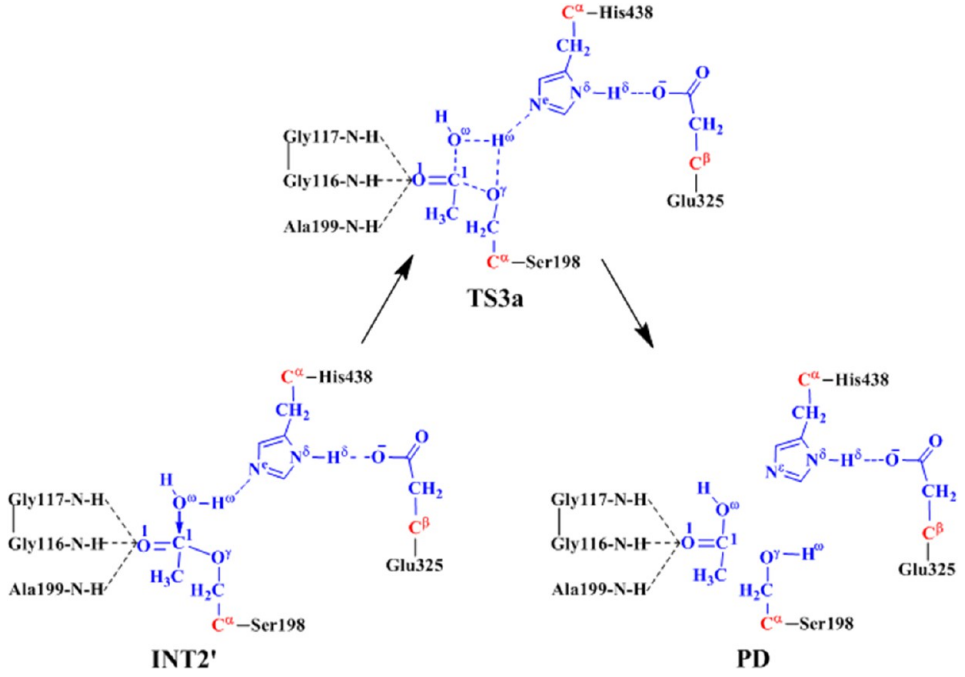

in Figure 2, $R_{C^1-O^\gamma}$ is decreased from 2.74 Å in the ES complex to 1.81 Å in TS1 and then to 1.62 Å in INT1. Simultaneously, $R_{H^\gamma-O^\gamma}$ is increased from 1.00 Å in the ES complex to 1.61 Å in TS1 and then to 1.70 Å in INT1, while $R_{H^\gamma-N^\epsilon}$ is decreased from 1.79 Å in the ES complex to 1.07 Å in TS1 and then to 1.06 Å in INT1. These structural variations indicate that the C^1-O^γ bond has formed and the hydroxyl H^γ atom has transferred to the N^ϵ atom of His438 in INT1. It is interesting to know the catalytic role of the oxyanion hole in this reaction step; although distance D_1 (between the hydrogen of NH group in Gly117 and O^1 of heroin) is increased from 1.88 Å in the ES complex to 1.99 Å in TS1 and then to 2.05 Å in INT1, distances D_2 (between the hydrogen of the NH group of Gly116 and O^1 of heroin) and D_3 (between the hydrogen of the NH group in Ala199 and O^1 of heroin) are decreased. In particular, D_3 = 2.54 Å in ES, 2.02 Å in TS1, and 1.94 Å in INT1. In other words, the interaction between the oxyanion hole and the negatively charged carbonyl oxygen (O^1) of heroin is strengthened, which helps to stabilize TS1 and INT1. Moreover, accompanied by transfer of the proton (H^γ) from the hydroxyl oxygen (O^γ) of Ser198 to the N^ϵ atom of His438, the imidazole ring of the His438 side chain becomes more and more positively charged. However, the developed positive charge on the imidazole ring of His438 can be stabilized by the negative charge of the Glu325 side chain, which is demonstrated by the shortened hydrogen bond distance between the carboxylate anion of Glu325 and the proton (H^δ) on N^δ of His438 ($H^\delta\cdots O$ distances in $N^\delta-H^\delta\cdots O$ hydrogen bonds of 1.66 Å in ES, 1.57 Å in TS1, and 1.56 Å in INT1).

Dissociation of 6-MAM from the Enzyme (step 2). In this reaction step, the C^1-O^2 bond is gradually broken while the proton (H^γ) transfers from N^ϵ of His438 to O^2, resulting in the dissociation of 6-MAM from the enzyme. This reaction step involves the breaking of the $N^\epsilon-H^\gamma$ and C^1-O^2 bonds and the formation of the O^2-H^γ bond. The nature of this reaction step can be represented by the changes in the $N^\epsilon-H^\gamma$ distance ($R_{N^\epsilon-H^\gamma}$), the C^1-O^2 distance ($R_{C^1-O^2}$), and the O^2-H^γ distance ($R_{O^2-H^\gamma}$). Thus, the reaction coordinate in the QM/MM calculations for this step was chosen as $R_{N^\epsilon-H^\gamma} + R_{C^1-O^2} - R_{O^2-H^\gamma}$. In the INT1 structure, the proton (H^γ) of the Ser198 side chain has been transferred to N^ϵ of His438 in reaction step 1 while distance $R_{O^\gamma-H^\gamma}$ between the O^γ atom of Ser198 and the H^γ atom of His438 is 1.70 Å, indicating a very strong hydrogen bond ($N^\epsilon-H^\gamma\cdots O^\gamma$) between the oxygen of the Ser198 side chain and the NH group of the His438 side chain. The distance ($R_{O^2-H^\gamma}$) between the H^γ atom and the leaving ester O^2 atom to which H^γ is about to be transferred is 2.73 Å. However, accompanied by an increase in $R_{C^1-O^2}$ (1.57 Å in INT1 and 1.86 Å in TS2), $R_{O^2-H^\gamma}$ gradually decreases (2.73 Å in INT1 and 2.48 Å in TS2). Our reaction-coordinate calculations reveal that it is a one-step reaction process consisting of two substeps. In the first substep, the C^1-O^2 bond is broken. In the second substep, the proton (H^γ) gradually transfers to O^2. It should be noted that the interaction between the oxyanion hole and the negatively charged carbonyl oxygen (O^1) of heroin is enhanced from INT1 to TS2, indicating that the oxyanion hole plays an important role in the stabilization of TS2. In addition, associated with these structural variations, the positive charge on the imidazole ring of His438 is decreased and, therefore, the hydrogen bond between the carboxylate anion of Glu325 and the proton (H^δ) of His438 is weakened during this reaction step ($N^\delta-H^\delta\cdots O$ distances of 1.56 Å in INT1, 1.54 Å in TS2, and 1.74 Å in INT2).

Nucleophilic Attack on the Carbonyl Carbon of Heroin by a Water Molecule (step 3). The generated reaction product 6-MAM was removed from the QM/MM-optimized geometry of INT2 discussed above to construct the initial structure of INT2′ that was then relaxed by performing the MD simulation. A water molecule that is close to the carbonyl carbon (C^1) of heroin was selected as the nucleophile and was included in the QM part of the QM/MM calculation. As shown in Figure 3,

dx.doi.org/10.1021/bi400709v | *Biochemistry* 2013, 52, 6467−6479

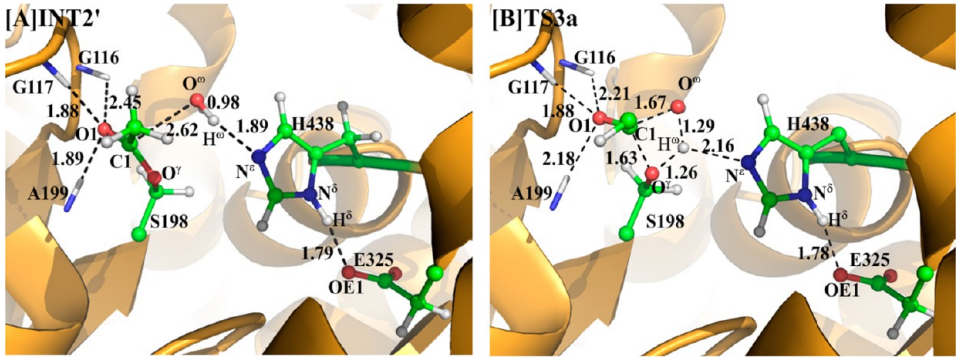

Figure 4. Geometries of INT2′ and TS3a optimized at the QM/MM(B3LYP/6-31G*:AMBER) level. The color code used here is the same as that in Figure 2.

two strong hydrogen bonds are formed between the carbonyl oxygen (O^1) and the oxyanion hole in the QM/MM-optimized geometry of INT2′.

The current nucleophilic attack process involves the breaking of the $O^{\omega}-H^{\omega}$ bond and the formation of the C^1-O^{ω} and $N^{\varepsilon}-H^{\omega}$ bonds (Scheme 2). Thus, distances $R_{O^{\omega}-H^{\omega}}$, $R_{C^1-O^{\omega}}$, and $R_{N^{\varepsilon}-H^{\omega}}$ were chosen to represent the reaction coordinate as $R_{O^{\omega}-H^{\omega}} - R_{C91-O^{\omega}} - R_{N^{\varepsilon}-H^{\omega}}$ in the QM/MM calculations for the current reaction step. During this reaction process, distance $R_{O^{\omega}-H^{\omega}}$ is increased from 0.98 Å in INT2′ to 1.43 Å in TS3 and then to 2.28 Å in INT3, while distances $R_{C^1-O^{\omega}}$ and $R_{N^{\varepsilon}-H^{\omega}}$ are decreased from 2.62 and 1.89 Å in INT2′ to 1.76 and 1.13 Å in TS3 and then to 1.49 and 1.05 Å in INT3, respectively. It is noteworthy that similar to reaction step 1 in the acylation stage, the interaction between the carbonyl oxygen (O^1) and the oxyanion hole is strengthened during this reaction step, which helps to stabilize TS3 and INT3. The developed positive charge on the imidazole ring of His438 is also stabilized by the strengthened hydrogen bond between the carboxylate anion of Glu325 and the proton (H^{δ}) of His438 ($N^{\delta}-H^{\delta}\cdots O$ distances of 1.79 Å in INT2′, 1.69 Å in TS3, and 1.61 Å in INT3).

In addition, we also tested the QM/MM reaction-coordinate calculations using alternative reaction coordinates in which two internuclear distances involving O^{γ} of Ser198 were added to the reaction coordinate. The first alternative reaction coordinate tested was $R_{C^1-O^{\gamma}} - R_{C^1-O^{\omega}} + R_{O^{\omega}-H^{\omega}} - R_{O^{\gamma}-H^{\omega}} - R_{N^{\varepsilon}-H^{\omega}}$. The QM/MM reaction-coordinate calculations using such a reaction coordinate may lead to a reaction pathway with the proton (H^{ω}) of the water molecule transferred to either N^{ε} of His438 (the main reaction pathway discussed above) or O^{γ} of Ser198 (an alternative reaction pathway). It turned out that the QM/MM calculations using this reaction coordinate led to exactly the same results as shown in Scheme 2 and Figure 3; i.e., the proton (H^{ω}) was still transferred to N^{ε} of His438 rather than O^{γ} of Ser198 during the reaction process.

Further, we performed the QM/MM reaction-coordinate calculations using $R_{C^1-O^{\gamma}} - R_{C^1-O^{\omega}} + R_{O^{\omega}-H^{\omega}} - R_{O^{\gamma}-H^{\omega}}$ as the reaction coordinate. This reaction coordinate involves the breaking of the C^1-O^{γ} and $O^{\omega}-H^{\omega}$ bonds and formation of the C^1-O^{ω} and $O^{\gamma}-H^{\omega}$ bonds. The QM/MM reaction-coordinate calculations using such a reaction coordinate may only lead to a reaction pathway (as shown in Scheme 3) with the proton (H^{ω}) transferred to O^{γ} of Ser198 during the nucleophilic attack of O^{ω} on C^1 of Ser198. In fact, the QM/MM reaction-coordinate calculations using this reaction coordinate led to an unfavorable, high-energy transition state structure, denoted as TS3a in Figure 4, with a four-membered ring (see below for the energetic results); we stopped the unnecessary further reaction-coordinate calculations after TS3a had been identified.

Dissociation between the Acetic Acid and Ser198 of BChE (step 4). As seen from Scheme 2, this reaction step involves the breaking of the C^1-O^{γ} and $N^{\varepsilon}-H^{\omega}$ bonds and the formation of the $O^{\gamma}-H^{\omega}$ bond. The changes in distances $R_{C^1-O^{\gamma}}$, $R_{N^{\varepsilon}-H^{\omega}}$, and $R_{O^{\gamma}-H^{\omega}}$ reflect the nature of this reaction step. Thus, the reaction coordinate $R_{C^1-O^{\gamma}} + R_{N^{\varepsilon}-H^{\omega}} - R_{O^{\gamma}-H^{\omega}}$ was set in the QM/MM calculations for this reaction step. In the formed intermediate INT3, $R_{O^{\gamma}-H^{\omega}}$ is 1.79 Å, indicating that a strong hydrogen bond has formed between the oxygen of the Ser198 side chain and the H^{ω} atom. As shown in Figure 3, $R_{C^1-O^{\gamma}}$ and $R_{N^{\varepsilon}-H^{\omega}}$ increase from 1.60 and 1.05 Å in INT3 to 1.85 and 1.14 Å in TS4 and then to 2.40 and 1.80 Å in PD, respectively, while $R_{O^{\gamma}-H^{\omega}}$ decreases from 1.79 Å in INT3 to 1.45 Å in TS4 and then to 1.00 Å in PD.

Roles of the Catalytic Triad and Oxyanion Hole. According to the reaction pathways described above that were examined by our pseudobond first-principles QM/MM-FE calculations, the catalytic triad and oxyanion hole of the enzyme are the most important factors in BChE-catalyzed hydrolysis of heroin to 6-MAM. The catalytic triad consists of Ser198, His438, and Glu325, in which Ser198 acts as a nucleophile in reaction step 1 to initiate the hydrolysis reaction, His438 serves as a general base that accepts the proton from the nucleophile to facilitate the two nucleophilic attack processes, i.e., reaction steps 1 and 3, and Glu325 helps to stabilize the transition states by strengthening the hydrogen bonding interaction with His438 throughout the hydrolysis reaction. The oxyanion hole consists of the backbone NH groups of Gly116, Gly117, and Ala199 and helps to stabilize the transition states throughout the hydrolysis reaction. On the basis of the QM/MM reaction-coordinate calculations, in the initial ES complex, the carbonyl oxygen (O^1) of heroin forms only two hydrogen bonds with the oxyanion hole: the of $N-H\cdots O^1$ hydrogen bond with the backbone NH group of Gly116 and the $N-H\cdots O^1$ hydrogen bond with the backbone NH group of Gly117. As shown in Figure 2B, the two $H\cdots O^1$ distances are all ~1.9 Å. In comparison, the $H\cdots O^1$ distance between the backbone NH group of Ala199 and the carbonyl oxygen (O^1) of heroin (~2.5 Å) is relatively longer. However, in rate-determining transition state TS2 (see below for the free energy profile) shown in Figure 2E, the hydrogen bond between the backbone NH group of Ala199 and the carbonyl oxygen (O^1) of heroin is strengthened significantly (with the $H\cdots O^1$ distance changing from ~2.5 to ~1.9 Å). For the other two hydrogen bonds with the backbone NH groups of Gly116 and Gly117, the changes in

dx.doi.org/10.1021/bi400709v | *Biochemistry* 2013, 52, 6467−6479

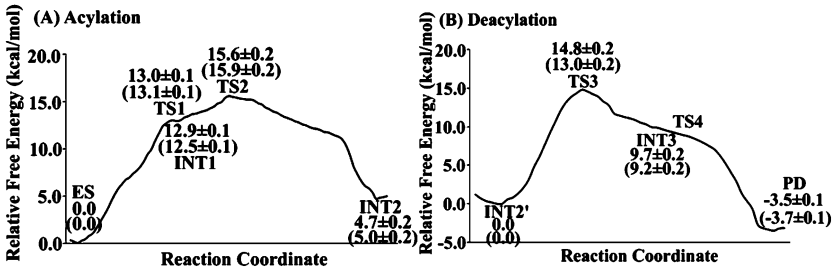

Figure 5. Free energy profile determined by the QM/MM-FE calculations for the acylation (A) and deacylation (B) stages of the reaction pathway. Given in parentheses are the relative free energies with the zero-point and thermal corrections for the QM subsystem. The QM/MM-FE calculations for all QM/MM-optimized geometries along the reaction path were performed at the B3LYP/6-31++G**:AMBER level.

the H···O[1] distances (~1.8 and ~2.0 Å, respectively) are relatively small during the hydrolysis reaction. All three hydrogen bonds stabilize the negative charge on the carbonyl oxygen (O[1]) of heroin that develops during the hydrolysis reaction. Thus, we can conclude that, for BChE-catalyzed hydrolysis of heroin, the catalytic triad initiates the reaction and the oxyanion hole helps to accelerate the reaction. The roles of the catalytic triad and oxyanion hole noted in the BChE-catalyzed hydrolysis of heroin are essentially similar to those observed in previous QM/MM reaction-coordinate calculations on acetylcholine (ACh) hydrolysis or other ester hydrolysis reactions catalyzed by either AChE[69,70] or BChE.[26,29,30] In fact, AChE and BChE have the same catalytic triad and oxyanion hole. The main difference between AChE and BChE exists in the size of the active site gorge, with BChE having a relatively larger active site gorge, resulting in different substrate selectivity.[71−78] With a larger active site gorge, BChE can accommodate relatively larger substrates than AChE can. For a common substrate such as ACh, the two enzymes are expected to follow the same fundamental reaction pathway,[26,29,48,70] but with different energy barriers.

Free Energy Profiles. The aforementioned QM/MM reaction-coordinate calculations at the B3LYP/6-31G*:AMBER level have revealed that the main reaction pathway consists of four reaction steps (steps 1 and 2 belong to the acylation stage and steps 3 and 4 to the deacylation stage) in the BChE-catalyzed hydrolysis of heroin to 6-MAM. For an alternative reaction pathway, the deacylation stage becomes a single reaction step (the third reaction step). Further, to determine the free energy profiles for the reaction pathways, we conducted the single-point QM/MM energy calculations with the QM part treated at the B3LYP/6-31++G** level for each QM/MM-optimized geometry along the minimal energy path. With regard to the results of the FEP calculations, the relative free energy of the reaction system was taken as the average of the "forward" and "backward" perturbation results in which the difference between the forward and backward perturbation results may represent the error bar of the FEP calculations.

Depicted in Figure 5 is the free energy profile calculated for the main reaction pathway by the QM/MM-FE calculations at the B3LYP/6-31++G**:AMBER level without the zero-point and thermal corrections for the QM subsystem, and depicted in Figure 6 is the free energy profile determined for the alternative third reaction step by using the same computational approach. The values in parentheses are the corresponding relative free energies including the zero-point and thermal corrections for the QM subsystem. The error bars given to the relative free energies in the figures are associated with the free energy differences between the forward and backward perturbation

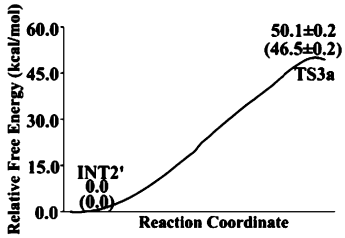

Figure 6. Free energy profile for the alternative pathway of the third reaction step according to the QM/MM-FE calculations. Given in parentheses are the relative free energies with the zero-point and thermal corrections for the QM subsystem. The QM/MM-FE calculations for all QM/MM-optimized geometries along the reaction path were performed at the B3LYP/6-31++G**:AMBER level.

calculations. The largest error bar was ±0.2 kcal/mol, suggesting that the FEP calculations converged well in terms of the number of FEP windows used.

As seen in Figure 6, the free energy barrier calculated for the alternative pathway of the third reaction step (deacylation) is as high as 46.5 ± 0.2 kcal/mol, and thus, this alternative reaction pathway can be ignored compared to the main reaction pathway. Therefore, in the discussion below, we focus on the free energy profile (Figure 5) calculated for the main reaction pathway.

As one can see in Figure 5, the calculated results reveal that the relative energy of TS2 is higher than that of TS1, indicating that the calculated overall free energy barrier for the entire acylation stage is the change in free energy from ES to TS2. Similarly, the higher energy of TS3 relative to that of TS4 indicates that the overall free energy barrier calculated for the deacylation is the change in free energy from INT2′ to TS3. According to the results, the free energy barrier for the acylation is higher than that for the deacylation, demonstrating that the free energy change associated with the structural transformation from ES to TS2 is rate-determining for the BChE-catalyzed hydrolysis of heroin to 6-MAM. Noteworthy is the fact that the energy barrier of the fourth step, i.e., dissociation of the acetic acid and Ser198, is only ~0.2 kcal/mol according to the potential energy surface calculated at the QM/MM(B3LYP/6-31G*:AMBER) level. The negligible energy barrier disappears according to the final QM/MM-FE calculations performed at the B3LYP/6-31++G**:AMBER level, suggesting that the final step of the enzymatic reaction is actually barrier-less after the FEP calculations.

Finally, we examined the basis set dependence of the QM/MM-FE calculations results for the rate-determining step associated with TS2 (i.e., the change in free energy from ES to TS2). When the basis set used in the QM part of the QM/

dx.doi.org/10.1021/bi400709v | Biochemistry 2013, 52, 6467−6479

MM calculations changed from 6-31+G* to 6-31++G**, the overall free energy barrier calculated for the rate-determining step (i.e., the change in free energy from ES to TS2) changed significantly from 13.8 ± 0.2 to 15.9 ± 0.2 kcal/mol, with a net change of 2.1 kcal/mol. However, when the basis set further changed from 6-31++G** to 6-311++G**, the calculated overall free energy barrier for the rate-determining step changed from 15.9 ± 0.2 to 16.1 ± 0.2 kcal/mol, with a net change of only 0.2 kcal/mol, suggesting that the 6-31++G** or 6-311++G** basis set is large enough. Therefore, the overall free energy barrier calculated for the rate-determining step associated with TS2 is 15.9 ± 0.2 kcal/mol (using the 6-31++G** basis set) or 16.1 ± 0.2 kcal/mol (using the 6-311++G** basis set). According to the reported experimental data,[14] k_{cat} = 540 min^{-1}, which is associated with an activation free energy of ∼16.2 kcal/mol at room temperature (25 °C) according to the conventional transition state theory.[79] The calculated free energy barrier of 15.9 ± 0.2 or 16.1 ± 0.2 kcal/mol is very close to the experimentally derived activation free energy of ∼16.2 kcal/mol, which suggests that the computational results are reasonable.

Insights from the Mechanistic Understanding for the Rational Design of Novel Therapeutic Agents. Currently used therapeutic treatments of heroin abuse all target opiate receptors. As noted above, the pharmacological function of heroin requires an activation process that transforms heroin into 6-MAM (the most active form), and BChE is the major enzyme responsible for this activation process. It might be interesting to develop a novel therapeutic treatment targeting the activation process, particularly BChE-catalyzed hydrolysis of heroin to 6-MAM. One possibility is to design a small molecule allosteric inhibitor that can significantly increase the free energy barrier for BChE-catalyzed hydrolysis of heroin to 6-MAM without significantly affecting the other functions of the enzyme. The desirable allosteric inhibitor should bind to a binding site (other than the active site), such as the well-known peripheral anionic site of BChE (around Asp70), so that it does not block the active site. The allosteric inhibitor should be designed to increase the overall free energy barrier, i.e., the change in free energy from ES to TS2 depicted in Figure 2. For the purpose of increasing the change in free energy from ES to TS2, one should aim to design an allosteric inhibitor that can more favorably stabilize the ES structure and less favorably stabilize (or destabilize) the TS2 structure.

For the practical design of an allosteric inhibitor, one may computationally test a variety of possible small molecules. For each of the possible small molecules, one may first computationally evaluate its binding affinity with the ES structure of BChE. If the small molecule is evaluated to have a high affinity with the ES structure, then one may further conduct QM/MM-FE calculations on the BChE-catalyzed hydrolysis of heroin in the presence of the small molecule to predict the free energy barrier (i.e., the change in free energy from ES to TS2). The small molecule predicted to significantly increase the free energy barrier may be recommended for wet experiments, including chemical synthesis and *in vitro* activity assays.

■ CONCLUSION

The first-principles QM/MM-FE calculations performed in this study have demonstrated the detailed reaction pathway for the BChE-catalyzed hydrolysis of heroin to 6-MAM. According to the QM/MM calculations, the whole reaction pathway for the BChE-catalyzed hydrolysis of heroin consists of four reaction steps. The reaction is initiated by the nucleophilic attack of the hydroxyl oxygen (O^{γ}) atom of the Ser198 side chain on the carbonyl carbon (C^1) of the 3-acetyl group of heroin, accompanied by the transfer of a proton (H^{γ}) from the Ser198 O^{γ} atom to the His438 N^{ε} atom. The tetrahedral INT1 is thus formed, in which the negatively charged carbonyl oxygen (O^1) is stabilized by the backbone NH groups of Gly116, Gly117, and Ala199 in the oxyanion hole. Subsequently, the C^1-O^2 bond is gradually broken while the proton (H^{γ}) is transferred from the His438 N^{ε} atom to the O^2 atom, leading to the formation of 6-MAM and the acyl−enzyme intermediate. The third reaction step is initiated by the nucleophilic attack of a water molecule on the carbonyl carbon (C^1) atom of the acyl−enzyme intermediate. This process is coupled with the transfer of a proton (H^{ω}) from the water oxygen (O^{ω}) to the His438 N^{ε} atom. Finally, the acetyl group is released with the regeneration of Ser198.

The calculated free energy profile reveals that the second transition state (TS2) should be the rate-determining transition state, and that the overall free energy barrier for the reaction should be the change in free energy from ES to TS2. The structural analysis reveals that the oxyanion hole plays an important role in the stabilization of rate-determining transition state TS2. The calculated overall free energy barrier of 15.9 ± 0.2 or 16.1 ± 0.2 kcal/mol is in good agreement with the experimentally derived activation free energy of ∼16.2 kcal/mol, suggesting that the mechanistic insights obtained from the QM/MM-FE calculations are reliable. The obtained structural and mechanistic insights could be valuable for use in the future rational design of a novel therapeutic strategy that aims to control heroin mechanism and, thus, treat heroin abuse.

■ AUTHOR INFORMATION

Corresponding Author

*Department of Pharmaceutical Sciences, College of Pharmacy, University of Kentucky, 789 S. Limestone St., Lexington, KY 40536. Telephone: (859) 323-3943. Fax: (859) 323-3575. E-mail: zhan@uky.edu.

Funding

This work was supported in part by the National Institutes of Health (Grants R01 DA035552, R01 DA032910, R01 DA013930, and R01 DA025100) and the National Science Foundation (Grant CHE-1111761). Y.Q. was supported by the China Scholarship Council.

Notes

The authors declare no competing financial interest.

■ ACKNOWLEDGMENTS

Y.Q. worked in C.-G.Z.'s laboratory for this project at the University of Kentucky as an exchange graduate student. We also acknowledge the Computer Center at the University of Kentucky for supercomputing time on a Dell X-series Cluster with 384 nodes or 4768 processors.

■ REFERENCES

(1) National Insititute on Drug Abuse (2013) The Science of Drug Abuse & Addiction (http://www.drugabuse.gov/publications/drugfacts/heroin).

(2) Oldendorf, W. H., Hyman, S., Braun, L., and Oldendorf, S. Z. (1972) Blood-brain barrier: Penetration of morphine, codeine, heroin, and methadone after carotid injection. *Science 178*, 984−986.

(3) Selley, D. E., Cao, C. C., Sexton, T., Schwegel, J. A., Martin, T. J., and Childers, S. R. (2001) mu Opioid receptor-mediated G-protein

activation by heroin metabolites: Evidence for greater efficacy of 6-monoacetylmorphine compared with morphine. *Biochem. Pharmacol. 62*, 447−455.
(4) Way, E. L., Kemp, J. W., Young, J. M., and Grassetti, D. R. (1960) The pharmacologic effects of heroin in relationship to its rate of biotransformation. *J. Pharmacol. Exp. Ther. 129*, 144−154.
(5) Way, E. L., Young, J. M., and Kemp, J. W. (1965) Metabolism of Heroin and Its Pharmacologic Implications. *Bull. Narc. 17*, 25−33.
(6) Goldberger, B. A., Cone, E. J., Grant, T. M., Caplan, Y. H., Levine, B. S., and Smialek, J. E. (1994) Disposition of heroin and its metabolites in heroin-related deaths. *J. Anal. Toxicol. 18*, 22−28.
(7) Eddy, N. B., and Howes, H. A. (1935) Studies of morphine, codeine and their derivatives. VIII. Monoacetyl- and diacetylmorphine their hydrogenated derivatives. *J. Pharmacol. Exp. Ther. 53*, 430−439.
(8) Wright, C. I., and Barbour, F. A. (1935) The respiratory effects of morphine, codeine and related substances IV. The effect of α-monoacetylmorphine, monoacetyldihydromorphine, diacetylmorphine (heroin) and diacetyldihydromorphine on the respiratory activity of the rabbit. *J. Pharmacol. Exp. Ther. 54*, 25−33.
(9) Lockridge, O., Mottershaw-Jackson, N., Eckerson, H. W., and La Du, B. N. (1980) Hydrolysis of diacetylmorphine (heroin) by human serum cholinesterase. *J. Pharmacol. Exp. Ther. 215*, 1−8.
(10) Andersen, J. M., Ripel, A., Boix, F., Normann, P. T., and Morland, J. (2009) Increased locomotor activity induced by heroin in mice: Pharmacokinetic demonstration of heroin acting as a prodrug for the mediator 6-monoacetylmorphine in vivo. *J. Pharmacol. Exp. Ther. 331*, 153−161.
(11) Inturrisi, C. E., Schultz, M., Shin, S., Umans, J. G., Angel, L., and Simon, E. J. (1983) Evidence from Opiate Binding Studies That Heroin Acts through Its Metabolites. *Life Sci. 33*, 773−776.
(12) Strandberg, J. J., Kugelberg, F. C., Alkass, K., Gustavsson, A., Zahlsen, K., Spigset, O., and Druid, H. (2006) Toxicological analysis in rats subjected to heroin and morphine overdose. *Toxicol. Lett. 166*, 11−18.
(13) Kamendulis, L. M., Brzezinski, M. R., Pindel, E. V., Bosron, W. F., and Dean, R. A. (1996) Metabolism of cocaine and heroin is catalyzed by the same human liver carboxylesterases. *J. Pharmacol. Exp. Ther. 279*, 713−717.
(14) Salmon, A. Y., Goren, Z., Avissar, Y., and Soreq, H. (1999) Human erythrocyte but not brain acetylcholinesterase hydrolyses heroin to morphine. *Clin. Exp. Pharmacol. Physiol. 26*, 596−600.
(15) Boix, F., Andersen, J. M., and Morland, J. (2013) Pharmacokinetic modeling of subcutaneous heroin and its metabolites in blood and brain of mice. *Addict. Biol. 18*, 1−7.
(16) Martin, W. R., and Fraser, H. F. (1961) A comparative study of physiological and subjective effects of heroin and morphine administered intravenously in postaddicts. *J. Pharmacol. Exp. Ther. 133*, 388−399.
(17) Nakamura, G. R., Thornton, J. I., and Noguchi, T. T. (1975) Kinetics of heroin deacetylation in aqueous alkaline solution and in human serum and whole blood. *J. Chromatogr. 110*, 81−89.
(18) Owen, J. A., and Nakatsu, K. (1983) Diacetylmorphine (Heroin) Hydrolases in Human-Blood. *Can. J. Physiol. Pharmacol. 61*, 870−875.
(19) Rook, E. J., Huitema, A. D., van den Brink, W., van Ree, J. M., and Beijnen, J. H. (2006) Pharmacokinetics and pharmacokinetic variability of heroin and its metabolites: Review of the literature. *Curr. Clin. Pharmacol. 1*, 109−118.
(20) Zhang, Y. K., Lee, T. S., and Yang, W. T. (1999) A pseudodond approach to combining quantum mechanical and molecular mechanical methods. *J. Chem. Phys. 110*, 46−54.
(21) Zhang, Y. K., Liu, H. Y., and Yang, W. T. (2000) Free energy calculation on enzyme reactions with an efficient iterative procedure to determine minimum energy paths on a combined ab initio QM/MM potential energy surface. *J. Chem. Phys. 112*, 3483−3492.
(22) Zhang, Y. K. (2005) Improved pseudobonds for combined ab initio quantum mechanical/molecular mechanical methods. *J. Chem. Phys. 122*, 024114.
(23) Zhang, Y. K. (2006) Pseudobond ab initio QM/MM approach and its applications to enzyme reactions. *Theor. Chem. Acc. 116*, 43−50.
(24) Liu, J. J., Hamza, A., and Zhan, C. G. (2009) Fundamental Reaction Mechanism and Free Energy Profile for (−)-Cocaine Hydrolysis Catalyzed by Cocaine Esterase. *J. Am. Chem. Soc. 131*, 11964−11975.
(25) Liu, J. J., Zhang, Y. K., and Zhan, C. G. (2009) Reaction Pathway and Free-Energy Barrier for Reactivation of Dimethylphosphoryl-Inhibited Human Acetylcholinesterase. *J. Phys. Chem. B 113*, 16226−16236.
(26) Chen, X., Fang, L., Liu, J., and Zhan, C.-G. (2011) Reaction Pathway and Free Energy Profile for Butyrylcholinesterase-Catalyzed Hydrolysis of Acetylcholine. *J. Phys. Chem. B 115*, 1315−1322.
(27) Chen, X., Zhao, X., Xiong, Y., Liu, J., and Zhan, C. G. (2011) Fundamental reaction pathway and free energy profile for hydrolysis of intracellular second messenger adenosine 3′,5′-cyclic monophosphate (cAMP) catalyzed by phosphodiesterase-4. *J. Phys. Chem. B 115*, 12208−12219.
(28) Liu, J. J., Zhao, X. Y., Yang, W. C., and Zhan, C. G. (2011) Reaction Mechanism for Cocaine Esterase-Catalyzed Hydrolyses of (+)- and (−)-Cocaine: Unexpected Common Rate-Determining Step. *J. Phys. Chem. B 115*, 5017−5025.
(29) Chen, X., Fang, L., Liu, J., and Zhan, C.-G. (2012) Reaction Pathway and Free Energy Profiles for Butyrylcholinesterase-Catalyzed Hydrolysis of Acetylthiocholine. *Biochemistry 51*, 1297−1305.
(30) Liu, J., and Zhan, C.-G. (2012) Reaction pathway and free energy profile for cocaine hydrolase-catalyzed hydrolysis of (−)-cocaine. *J. Chem. Theory Comput. 8*, 1426−1435.
(31) Wei, D. H., Lei, B. L., Tang, M. S., and Zhan, C. G. (2012) Fundamental Reaction Pathway and Free Energy Profile for Inhibition of Proteasome by Epoxomicin. *J. Am. Chem. Soc. 134*, 10436−10450.
(32) Yao, Y., Liu, J., and Zhan, C.-G. (2012) Why does the G117H mutation considerably improve the activity of human butyrylcholinesterase against sarin? Insights from quantum mechanical/molecular mechanical free energy calculations. *Biochemistry 51*, 8980−8992.
(33) Li, D., Huang, X., Lin, J., and Zhan, C.-G. (2013) Catalytic mechanism of cytochrome P450 for N-methylhydroxylation of nicotine: Reaction pathways and regioselectivity of the enzymatic nicotine oxidation. *Dalton Trans. 42*, 3812−3820.
(34) Wei, D., Huang, X., Liu, J., Tang, M., and Zhan, C.-G. (2013) Reaction Pathway and Free Energy Profile for Papain-Catalyzed Hydrolysis of N-Acetyl-Phe-Gly 4-Nitroanilide. *Biochemistry 52*, 5145−5154.
(35) Zheng, F., Yang, W. C., Ko, M. C., Liu, J. J., Cho, H., Gao, D. Q., Tong, M., Tai, H. H., Woods, J. H., and Zhan, C. G. (2008) Most efficient cocaine hydrolase designed by virtual screening of transition states. *J. Am. Chem. Soc. 130*, 12148−12155.
(36) Wandhammer, M., Carletti, E., Van der Schans, M., Gillon, E., Nicolet, Y., Masson, P., Goeldner, M., Noort, D., and Nachon, F. (2011) Structural study of the complex stereoselectivity of human butyrylcholinesterase for the neurotoxic V-agents. *J. Biol. Chem. 286*, 16783−16789.
(37) Balchin, E., Malcolme-Lawes, D. J., Rowe, M. D., Smith, J. A. S., Bearpark, M. J., Steed, J. W., Wu, W., Horsewill, A. J., and Stephenson, D. (2004) The unusual solid state structure of heroin hydrochloride monohydrate and its selective detection using NQR spectroscopy. *New J. Chem. 28*, 1309−1314.
(38) Frisch, M. J., Trucks, G. W., Schlegel, H. B., Scuseria, G. E., Robb, M. A., Cheeseman, J. R., Montgomery, J. A., Jr., Vreven, T., Kudin, K. N., Burant, J. C., Millam, J. M., Iyengar, S. S., Tomasi, J., Barone, V., Mennucci, B., Cossi, M., Scalmani, G., Rega, N., Petersson, G. A., Nakatsuji, H., Hada, M., Ehara, M., Toyota, K., Fukuda, R., Hasegawa, J., Ishida, M., Nakajima, T., Honda, Y., Kitao, O., Nakai, H., Klene, M., Li, X., Knox, J. E., Hratchian, H. P., Cross, J. B., Bakken, V., Adamo, C., Jaramillo, J., Gomperts, R., Stratmann, R. E., Yazyev, O., Austin, A. J., Cammi, R., Pomelli, C., Ochterski, J. W., Ayala, P. Y., Morokuma, K., Voth, G. A., Salvador, P., Dannenberg, J. J., Zakrzewski, V. G., Dapprich, S., Daniels, A. D., Strain, M. C., Farkas, O., Malick, D.

K., Rabuck, A. D., Raghavachari, K., Foresman, J. B., Ortiz, J. V., Cui, Q., Baboul, A. G., Clifford, S., Cioslowski, J., Stefanov, B. B., Liu, G., Liashenko, A., Piskorz, P., Komaromi, I., Martin, R. L., Fox, D. J., Keith, T., Al-Laham, M. A., Peng, C. Y., Nanayakkara, A., Challacombe, M., Gill, P. M. W., Johnson, B., Chen, W., Wong, M. W., Gonzalez, C., and Pople, J. A. (2004) *Gaussian 03*, version C.02, Gaussian, Inc., Wallingford, CT.

(39) Bayly, C. I., Cieplak, P., Cornell, W. D., and Kollman, P. A. (1993) A well-behaved electrostatic potential based method using charge restraints for deriving atomic charges: The resp model. *J. Phys. Chem. 97*, 10269−10280.

(40) Cieplak, P., Cornell, W. D., Bayly, C., and Kollman, P. A. (1995) Application of the multimolecule and multiconformational resp methodology to biopolymers: Charge derivation for DNA, RNA, and proteins. *J. Comput. Chem. 16*, 1357−1377.

(41) Case, D. A., Darden, T. A., Cheatham, T. E., Simmerling, C. L., Wang, J., Duke, R. E., Luo, R., Merz, K. M., Wang, B., Pearlman, D. A., Crowley, M., Brozell, S., Tsui, V., Gohlke, H., Mongan, J., Hornak, V., Cui, G., Beroza, P., Schafmeister, C., Caldwell, J. W., Ross, W. S., and Kollman, P. A. (2010) *AMBER11*, University of California, San Francisco.

(42) Morris, G. M., Goodsell, D. S., Halliday, R. S., Huey, R., Hart, W. E., Belew, R. K., and Olson, A. J. (1998) Automated docking using a Lamarckian genetic algorithm and an empirical binding free energy function. *J. Comput. Chem. 19*, 1639−1662.

(43) Duan, Y., Wu, C., Chowdhury, S., Lee, M. C., Xiong, G., Zhang, W., Yang, R., Cieplak, P., Luo, R., Lee, T., Caldwell, J., Wang, J., and Kollman, P. (2003) A point-charge force field for molecular mechanics simulations of proteins based on condensed-phase quantum mechanical calculations. *J. Comput. Chem. 24*, 1999−2012.

(44) Wang, J. M., Wolf, R. M., Caldwell, J. W., Kollman, P. A., and Case, D. A. (2004) Development and testing of a general Amber force field. *J. Comput. Chem. 25*, 1157−1174.

(45) Jorgensen, W. L., Chandrasekhar, J., Madura, J. D., Impey, R. W., and Klein, M. L. (1983) Comparison of Simple Potential Functions for Simulating Liquid Water. *J. Chem. Phys. 79*, 926−935.

(46) Toukmaji, A., Sagui, C., Board, J., and Darden, T. (2000) Efficient particle-mesh Ewald based approach to fixed and induced dipolar interactions. *J. Chem. Phys. 113*, 10913−10927.

(47) Ryckaert, J. P., Ciccotti, G., and Berendsen, H. J. C. (1977) Numerical-Integration of Cartesian Equations of Motion of a System with Constraints: Molecular-Dynamics of N-Alkanes. *J. Comput. Phys. 23*, 327−341.

(48) Zhou, Y., Wang, S., and Zhang, Y. (2010) Catalytic reaction mechanism of acetylcholinesterase determined by Born-Oppenheimer ab initio QM/MM molecular dynamics simulations. *J. Phys. Chem. B 114*, 8817−8825.

(49) Lee, C., Yang, W., and Parr, R. G. (1988) Development of the Colle-Salvetti correlation-energy formula into a functional of the electron density. *Phys. Rev. B 37*, 785−789.

(50) Becke, A. D. (1993) Density-Functional Thermochemistry. 3. The Role of Exact Exchange. *J. Chem. Phys. 98*, 5648−5652.

(51) Stephens, P. J., Devlin, F. J., Chabalowski, C. F., and Frisch, M. J. (1994) Ab-Initio Calculation of Vibrational Absorption and Circular-Dichroism Spectra Using Density-Functional Force-Fields. *J. Phys. Chem. 98*, 11623−11627.

(52) Case, D. A., Darden, T. A., Cheatham, T. E., Simmerling, C. L., Wang, J., Duke, R. E., Luo, R., Merz, K. M., Wang, B., Pearlman, D. A., Crowley, M., Brozell, S., Tsui, V., Gohlke, H., Mongan, J., Hornak, V., Cui, G., Beroza, P., Schafmeister, C., Caldwell, J. W., Ross, W. S., and Kollman, P. A. (2004) *AMBER8*, University of California, San Francisco.

(53) Smith, A. J., Muller, R., Toscano, M. D., Kast, P., Hellinga, H. W., Hilvert, D., and Houk, K. N. (2008) Structural reorganization and preorganization in enzyme active sites: Comparisons of experimental and theoretically ideal active site geometries in the multistep serine esterase reaction cycle. *J. Am. Chem. Soc. 130*, 15361−15373.

(54) Ramalho, T. C., Tanos, C. C., Renno, M. N., Guimaraes, A. P., da Cunha, E. F., and Kuca, K. (2010) Development of new acetylcholinesterase reactivators: Molecular modeling versus in vitro data. *Chem.-Biol. Interact. 185*, 73−77.

(55) Chandrasekhar, J., Smith, S. F., and Jorgensen, W. L. (1984) Sn2 Reaction Profiles in the Gas-Phase and Aqueous-Solution. *J. Am. Chem. Soc. 106*, 3049−3050.

(56) Kollman, P. (1993) Free-Energy Calculations: Applications to Chemical and Biochemical Phenomena. *Chem. Rev. 93*, 2395−2417.

(57) Beveridge, D. L., and DiCapua, F. M. (1989) Free energy via molecular simulation: Applications to chemical and biomolecular systems. *Annu. Rev. Biophys. Biophys. Chem. 18*, 431−492.

(58) Acevedo, O., and Jorgensen, W. L. (2010) Advances in Quantum and Molecular Mechanical (QM/MM) Simulations for Organic and Enzymatic Reactions. *Acc. Chem. Res. 43*, 142−151.

(59) Acevedo, O., and Jorgensen, W. L. (2006) Cope elimination: Elucidation of solvent effects from QM/MM simulations. *J. Am. Chem. Soc. 128*, 6141−6146.

(60) Acevedo, O., and Jorgensen, W. L. (2005) Influence of inter- and intramolecular hydrogen bonding on Kemp decarboxylations from QM/MM simulations. *J. Am. Chem. Soc. 127*, 8829−8834.

(61) Alexandrova, A. N., Rothlisberger, D., Baker, D., and Jorgensen, W. L. (2008) Catalytic mechanism and performance of computationally designed enzymes for Kemp elimination. *J. Am. Chem. Soc. 130*, 15907−15915.

(62) Guimaraes, C. R., Udier-Blagovic, M., and Jorgensen, W. L. (2005) Macrophomate synthase: QM/MM simulations address the Diels-Alder versus Michael-Aldol reaction mechanism. *J. Am. Chem. Soc. 127*, 3577−3588.

(63) Guimaraes, C. R., Boger, D. L., and Jorgensen, W. L. (2005) Elucidation of fatty acid amide hydrolase inhibition by potent α-ketoheterocycle derivatives from Monte Carlo simulations. *J. Am. Chem. Soc. 127*, 17377−17384.

(64) Zhang, W., Hou, T. J., Qiao, X. B., Huai, S., and Xu, X. J. (2004) Binding affinity of hydroxamate inhibitors of matrix metalloproteinase-2. *J. Mol. Model. 10*, 112−120.

(65) Udier-Blagovic, M., Tirado-Rives, J., and Jorgensen, W. L. (2004) Structural and energetic analyses of the effects of the K103N mutation of HIV-1 reverse transcriptase on efavirenz analogues. *J. Med. Chem. 47*, 2389−2392.

(66) Jarmula, A., Cieplak, P., Les, A., and Rode, W. (2003) Relative free energies of binding to thymidylate synthase of 2- and/or 4-thio and/or 5-fluoro analogues of dUMP. *J. Comput.-Aided Mol. Des. 17*, 699−710.

(67) Danciulescu, C., Nick, B., and Wortmann, F. J. (2004) Structural stability of wild type and mutated α-keratin fragments: Molecular dynamics and free energy calculations. *Biomacromolecules 5*, 2165−2175.

(68) Funahashi, J., Sugita, Y., Kitao, A., and Yutani, K. (2003) How can free energy component analysis explain the difference in protein stability caused by amino acid substitutions? Effect of three hydrophobic mutations at the 56th residue on the stability of human lysozyme. *Protein Eng. 16*, 665−671.

(69) Zhang, Y. K., Kua, J., and McCammon, J. A. (2002) Role of the catalytic triad and oxyanion hole in acetylcholinesterase catalysis: An ab initio QM/MM study. *J. Am. Chem. Soc. 124*, 10572−10577.

(70) Polyakov, I. V., Grigorenko, B. L., Moskovsky, A. A., Pentkovski, V. M., and Nemukhin, A. V. (2013) Towards quantum-based modeling of enzymatic reaction pathways: Application to the acetylholinesterase catalysis. *Chem. Phys. Lett. 556*, 251−255.

(71) Mesulam, M. M., Guillozet, A., Shaw, P., Levey, A., Duysen, E. G., and Lockridge, O. (2002) Acetylcholinesterase knockouts establish central cholinergic pathways and can use butyrylcholinesterase to hydrolyze acetylcholine. *Neuroscience 110*, 627−639.

(72) Masson, P., Bec, N., Froment, M. T., Nachon, F., Balny, C., Lockridge, O., and Schopfer, L. M. (2004) Rate-determining step of butyrylcholinesterase-catalyzed hydrolysis of benzoylcholine and benzoylthiocholine: Volumetric study of wild-type and D70G mutant behaviour. *Eur. J. Biochem. 271*, 1980−1990.

(73) Mattes, C., Bradley, R., Slaughter, E., and Browne, S. (1996) Cocaine and butyrylcholinesterase (BChE): Determination of enzymatic parameters. *Life Sci. 58*, Pl257−Pl261.
(74) Masson, P., Froment, M. T., Fortier, P. L., Visicchio, J. E., Bartels, C. F., and Lockridge, O. (1998) Butyrylcholinesterase-catalysed hydrolysis of aspirin, a negatively charged ester, and aspirin-related neutral esters. *Biochim. Biophys. Acta 1387*, 41−52.
(75) Amitay, M., and Shurki, A. (2011) Hydrolysis of organophosphate compounds by mutant butyrylcholinesterase: A story of two histidines. *Proteins 79*, 352−364.
(76) Dvir, H., Silman, I., Harel, M., Rosenberry, T. L., and Sussman, J. L. (2010) Acetylcholinesterase: From 3D structure to function. *Chem.-Biol. Interact. 187*, 10−22.
(77) Vellom, D. C., Radic, Z., Li, Y., Pickering, N. A., Camp, S., and Taylor, P. (1993) Amino acid residues controlling acetylcholinesterase and butyrylcholinesterase specificity. *Biochemistry 32*, 12−17.
(78) Fang, L., Pan, Y., Muzyka, J., and Zhan, C.-G. (2011) Active site gating and substrate specificity of butyrylcholinesterase and acetylcholinesterase: Insights from molecular dynamics simulations. *J. Phys. Chem. B 115*, 8797−8805.
(79) Alvarez-Idaboy, J. R., Galano, A., Bravo-Perez, G., and Ruiz, M. E. (2001) Rate constant dependence on the size of aldehydes in the NO_3 + aldehydes reaction. An explanation via quantum chemical calculations and CTST. *J. Am. Chem. Soc. 123*, 8387−8395.